

# Keysight Technologies

## Electromagnetic Simulations at the Nanoscale: EMPro Modeling and Comparison to SMM Experiments

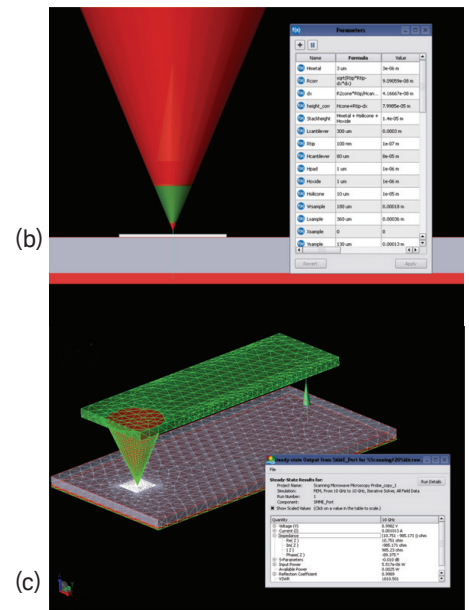
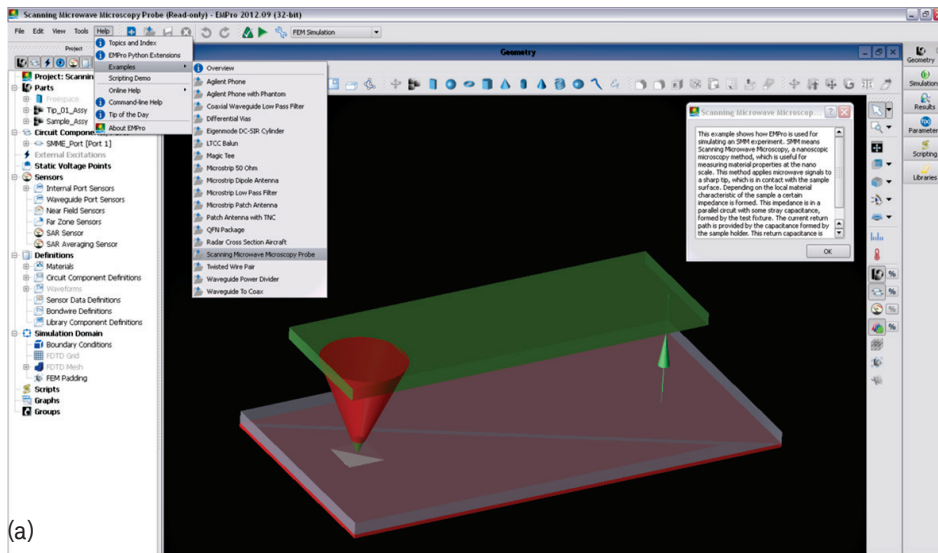
### Application Note

#### Introduction

In this application note, we describe electromagnetic (EM) simulations using Keysight Technologies' EMPro software<sup>1</sup> to support the interpretation of scanning microwave microscope (SMM) experiments. The SMM is a new scanning probe microscope that combines the electromagnetic measurement capabilities of a microwave Performance Network Analyzer (PNA) with the nanometer-resolution and Angstrom-scale positioning capabilities of an atomic force microscope (AFM).

Scanning microwave microscopy is a technique for measuring reflection scattering parameters and corresponding electric properties of materials at the nanoscale in the frequency range of 1–20GHz. Using EMPro, we modeled both the macroscopic AFM tip holder and the nanometric AFM tip in contact with a three-layer stack sample using the Finite Element Method (FEM). For this, 3D computer-aided drawings (CAD) of the tip holder and the tip-sample system were imported into EMPro. The electromagnetic field distribution and the complex impedance values of the sample were calculated and the corresponding reflection scattering parameters were determined at different frequencies. The EMPro modeling results were then compared to experimental SMM data, including complex impedance values of a standard calibration sample. A reasonable alignment between model and experiment was observed within 20% accuracy for the capacitance data.

Further applications of EMPro modeling are also presented in this application note, including the investigation of an oxide layer on top of a semiconductor and a Pt-SiO<sub>2</sub> cross-structure. The electromagnetic field distribution and corresponding complex impedance values were calculated with EMPro and compared to SMM measurements.



‘Setting up the SMM simulation in EMPro’ (a) The SMM project can be found in the Help/Examples menu. The examples are read-only files so it is useful to save a copy of the project for modifications. (b) The parameter menu is selected with each parameter having its own short description. Parameters that are related to geometric objects are numbered from 1 upwards, while parameters intended for modifications are labeled by zero. (c) Meshing of the tip-sample and numerical results, including complex impedance values (encircled in red). The simulations presented here are single-frequency simulations, but frequency sweeps are also possible. The second submenu provides several global parameters to control the meshing algorithm, while the third submenu allows selection of a direct or iterative solving strategy (here, iterative solving and quadratic base functions were used). Meshing can be controlled by individual mesh settings (which are independent for every part and include initial mesh size and meshing priority) and global mesh settings. Setting individual initial mesh sizes can help optimize the simulation time; different meshing priorities are useful to avoid meshing errors at overlapping areas (e.g., contact points). After setting the initial meshing, the refinement process starts. The mesh is iteratively refined and for every mesh a simulation result is calculated. The difference of the reflection coefficient of two consecutive simulations acts as the refinement exit criterion and a particular value can be preset. Regarding simulation time and memory, it took roughly 5 minutes on a standard desktop PC with a dual-core processor and 4GB RAM; the memory usage was roughly 2GB.

## Methods

All EMPro simulations were carried out in full-wave EM simulations. There are two simulation engines available in EMPro: Finite Element Method (FEM) and Finite Difference Time Domain (FDTD). Here, we used FEM simulations because of the availability of waveguide ports, which are useful for the examination of components with unknown wave propagation modes, and because of the flexible meshing algorithms of the FEM solution. The first step in setting up an EMPro model is to create the 3D geometry and define the materials and corresponding properties. The 3D model can be either created by using different low-level geometric forms (e.g., cylinders, cuboids, or frustums) or by importing a 3D CAD model (several file formats are accepted).

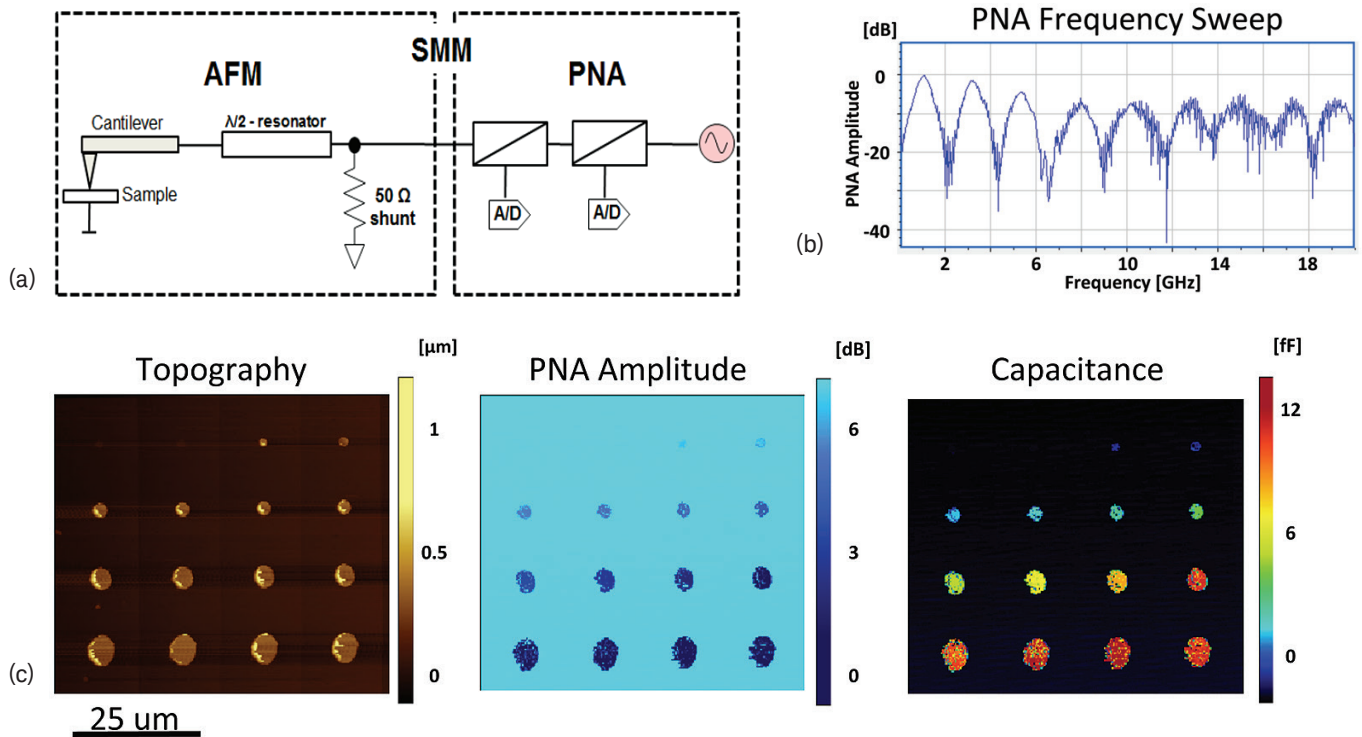
In this application note, we show the modeling of two different parts of the experimental setup that have significantly different length scales. Firstly, the macroscopic SMM nose cone was modeled, which is roughly a centimeter wide. The

nose cone consists of the AFM tip holder and the connection of the RF cable to the AFM tip. The modeling of the nose cone reveals information on the overall measurement setting and the various impedance matching properties of the connectors and cables. Secondly, the nanoscopic AFM tip was modeled that is sampling the device under test (i.e., the sample). The probe tip is roughly 10–100nm in diameter. From the nanoscopic tip-sample simulation we derived the reflection scattering parameters and corresponding complex impedance values of the tip-sample system. Those values were compared to SMM experiments of the capacitance calibration sample and a reasonable agreement was observed.

The nanoscopic tip-sample simulations are relevant for materials science investigations and the quantitative evaluation of complex impedance properties can be applied to various samples, including semiconductor circuits, energy materials, or biological cells and membranes. The SMM nose cone simulation particularly helps in understanding the macroscopic

measurement setting, including the analysis of stray capacitances from the cantilever and the overall sample. The separation of the modeling into a macroscopic part (i.e., the nose cone) and a nanoscopic part (i.e., the local tip-sample interaction) also avoids excessive computation requirements.

Details on the SMM experiments are given in the inbox ‘SMM experiments’, while details on the EMPro simulations are given in the inbox ‘Setting up the SMM simulation in EMPro’. Two application results of EMPro are presented: (1) the electromagnetic field distribution and attenuation was calculated for oxide layers with different thicknesses on a semiconductor sample, and (2) a cross-structure of a platinum metal and silicon oxide (Pt-SiO<sub>2</sub>) was modeled and both electromagnetic fields and corresponding impedance values were compared with SMM measurements. Both the qualitative E-field distribution and the quantitative impedance values agreed well with the experiments.



**'SMM experiments'** (a) In scanning microwave microscopy (SMM), a performance network analyzer (PNA) is interfaced with a standard atomic force microscope (AFM) to perform microwave network analysis at the nanoscale with frequencies ranging from 1–20GHz. The microwave signal generated by the PNA is transmitted via a coaxial cable to a conductive AFM tip. By comparing the incident RF signal to the back-reflected signal, the S11 network parameters are extracted by the PNA. A half-wavelength coaxial resonator in parallel with a 500 $\Omega$  shunt provides highest sensitivity for the SMM measurement. Thereby, minute variations around the load impedance can be measured, including calibrated capacitance values and semi-quantitative estimations of the resistance (i.e., complex impedance). With standard SMM settings, typically capacitances as small as 1aF can be measured. (b) PNA sweep over the full frequency range of 1–20GHz showing periodic notches every 2GHz with high measurement sensitivity typically used for SMM experiments. (c) Capacitance calibration: a standardized sample of small capacitor plates is used to transfer PNA amplitude values into absolute capacitance values ranging from roughly 0.1–10fF. The capacitance calibration sample is a three-layer stack sample of doped silicon, silicon oxide, and gold pads acting as small capacitors. The topographical image is acquired simultaneously to the complex S11 reflection parameters and displayed as PNA amplitude and PNA phase images. From the complex S11 data, calibrated capacitance and resistance images can be derived.<sup>2</sup>

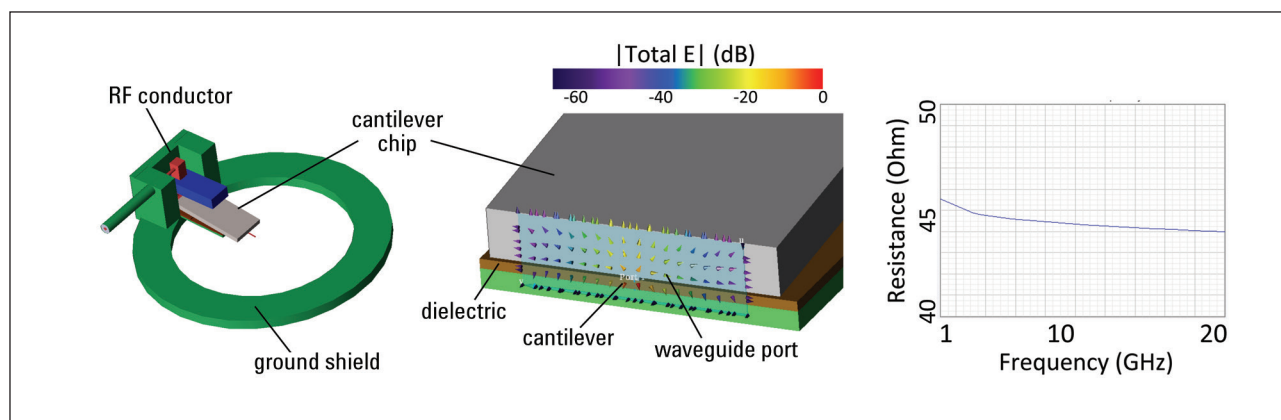


Figure 1. Macroscopic simulation of the SMM nose cone component. (a) Basic geometric model of the electrically relevant parts of the nose cone. The coaxial resonator cable and the cantilever were selected as the two ports for the modeling. Both ports are modeled as discrete voltage sources. (b) Waveguide structure showing the dielectric chip, the metallic cantilever, and the nose cone dielectric and ground. The two-dimensional port simulation was used to estimate the wave propagation modes and it behaves similarly to a 50 Ohm micro-strip transmission line. (c) From the above simulation, the wave impedance was calculated as a function of frequency ranging from 1–20 GHz. The SMM nose cone simulation is only required for the evaluation of the macroscopic stray capacitance and typically the calculation is not necessary for nanoscale studies. Hence, it is not included in the EMPro SMM project.

## Results and Discussion

Figure 1a shows a sketch of the nose cone, which is the macroscopic SMM component. The model includes the cantilever, the electrical transmission line, a coaxial resonator, and a metal housing that acts as an electrical shield. The nose cone connects the PNA with the AFM and the microwave signal is delivered to a conductive metal cantilever. It is engineered to provide consistent, stable, and low-loss microwave connection to the tip.

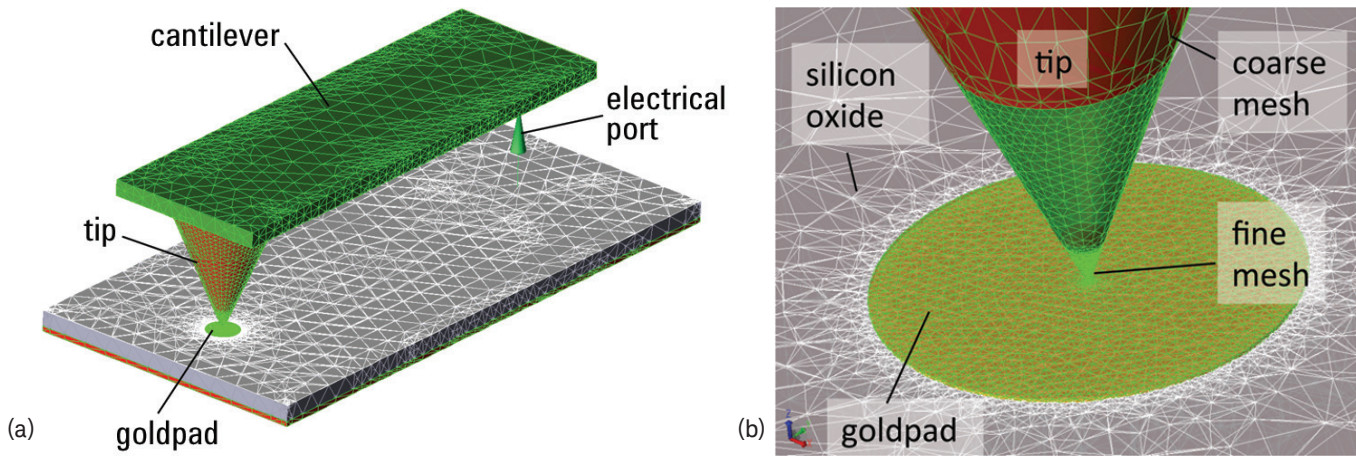
Based on the 3D CAD model, we examined the scattering parameters, including transmission between the PNA and cantilever as well as reflection properties at the tip-sample interface. For this, the CAD file was imported into EMPro and the electromagnetic field distribution was calculated. Based on the proper definitions of the ports, complex impedance values and reflection scattering coefficients were derived from the EM-field using standard EMPro procedures. Figure 1b shows the electric field distribution of a two-dimensional port simulation in order to examine the waveguide behavior of the cantilever / nose cone interface. The electric field distribution follows standard micro-strip transmission line behavior. From the simulation, the wave impedance was calculated at different frequencies and plotted in Figure 1c.

Between 1–20GHz, a nearly constant impedance around 50Ohm is obtained, which is in line with conventional RF circuitry, cables, and instruments. Based on the macroscopic evaluation of the SMM nose cone, the stray capacitance between the cantilever holder and the overall sample can be calculated and used to refine the measurement analysis. Here, the stray capacitance was subtracted from the SMM measurement results and a local analysis of the complex tip-sample impedance was pursued.<sup>3</sup> However, for standard nanoscale SMM studies the macroscopic nose cone modeling can be abandoned and only local tip-samples models can be investigated. Therefore, the macroscopic SMM nose cone model is not included in the EMPro project.

Figure 2 shows the nanoscopic tip-sample simulation that is also included as an SMM example project in EMPro. The inbox ‘Setting up the SMM simulation in EMPro’ gives an overview of proper meshing and parameter optimization. The project includes the probe tip in contact with three layers of different materials (metal, oxide, and semiconductor). Parameterization was used in order to create a flexible model of the tip-sample geometry. This allows simple adaptation of key dimensions such as probe tip radius or oxide thickness of the sample. In particular,

EMPro provides a parameter list for every simulation project, allowing the creation of various variable dimensions. For every geometric object (e.g., AFM tip, cantilever), separate parameters for the position (x, y, and z coordinates) and the key dimensions (e.g., diameter, thickness) were created. Also, mutual dependencies of the parameters were included as mathematical terms (e.g.,  $\text{length1} = \text{length2} + 0.5 \times \text{length3}$ ; the length describes the distance of the tip from the surface; for details, refer to the parameter descriptions in EMPro). Therefore, it is easily possible, for instance, to change the oxide thickness of the three-layer stack sample without affecting the contact condition between tip and sample.

Figure 2a shows the simulation of the AFM tip (including the cantilever) in contact with the three-layer stack sample of a semiconductor material (doped silicon), an oxide (silicon oxide), and a circularly shaped metal pad (gold pad). This sample is typically used in SMM capacitance and complex impedance calibration experiments and is a good starting point for more complex sample simulations. There are two kinds of meshes involved in Figure 2a. Surface meshing (green) was used for well-conducting mate-



Model	Oxide thickness (nm)	Gold pad diameter (um)	Complex impedance 10 GHz, EMPro	Capacitance (fF), EMPro	Capacitance (fF), SMM
1	100	1	0.7-j41.1 kOhm	0.39	0.3
2	100	2	0.4-j12.0 kOhm	1.3	1.1
3	100	6	0.1-j1.5 kOhm	10.6	9.8
(c) 4	100	10	0.09-j0.6 kOhm	28.4	27.1

rials (e.g., metals like the cantilever, tip, and gold pad) and volume meshing (white) was used for semiconductor materials and dielectrics (e.g., the doped silicon and the silicon oxide). Mainly based on material conductivity, the meshing algorithm decides automatically for each part of the model which kind of meshing to use. The conducting metal parts were treated as equipotential surfaces corroborated by the fact that the spatial dimensions of the model are small (few hundred micrometers length of the cantilever) in comparison to the wavelength of the electrical signals (on the order of centimeters at GHz). Therefore, the electrical excitation was set to a discrete voltage source connected to the cantilever (positive pole) and the bottom of the sample (negative pole). In Figure 2a, the source is represented by the green arrow labeled as electrical port.

Figure 2b gives a more detailed view of the tip in contact with the circularly shaped gold pad of 10 $\mu$ m diameter. Numerical results obtained from the EMPro simu-

lation are given in the table in Figure 2c, including capacitance and resistance values as calculated from complex impedance values at 10GHz. Four different gold pads with diameters ranging from 1–10 $\mu$ m were simulated and complex impedance values evaluated. For proper comparison to experimental SMM measurements the cantilever stray capacitance was subtracted from the total impedance. The last column in the table also lists the calibrated capacitance values as derived from SMM measurements of the same sample, including gold pads of 1–10 $\mu$ m in diameter.<sup>3, 4</sup> For experimental details, please refer to the inbox ‘SMM experiments’ showing a calibrated capacitance image of this sample. From the experimental SMM image the capacitance values were derived for the differently sized gold pads, assuming a parallel plate capacitor model as included in the current SMM measurement software.<sup>3</sup> The measured capacitance values agree with the simulations within 20%, which is currently given as the measurement accuracy of SMM. From the

SMM experiments, the resistance can also be estimated semi-quantitatively and the modeled resistance values agree with the experimental ones qualitatively.<sup>2</sup>

Figure 3 shows the electric field distribution of the AFM tip and the cantilever in contact with a three-layer stack sample.<sup>5</sup> The sample consists of a perfect electrical conductor (PEC) plane as bottom layer (i.e., an ideal metal), a doped silicon chip of 500 $\mu$ m thickness, and a smaller region of 50nm thick silicon oxide (SiO<sub>2</sub>). The dopant density of the silicon is set to medium values (~10<sup>17</sup> atoms/cm<sup>3</sup>), which results in a quite good, but not perfect conductivity. Therefore, there is also some electric field distribution obtained in the doped silicon.

Figure 3a shows the magnitude of the lateral electric field distribution on the silicon surface. Due to the cantilever, the field is not decaying symmetrically around the tip. In Figure 3b, the magnitude of the electric field is plotted into a vertical cut plane. The logarithmic color coding of the E-field values is adapted such that the electric field is also visible inside the silicon. In Figures 3c and 3d, a closer look at the E-field distribution on the surface of the 50nm thick silicon oxide is shown. While the field plots in Figures 3a and 3b are done with the advanced visualization tool of EMPro, the field data in Figures 3c and 3d are drawn by a specific surface field sensor assigned to the silicon oxide surface. The E-field data can thereby be plotted directly in the geometry window.

Figure 4 shows a first example of the use of EMPro to support SMM measurements. A closer look at the E-field distribution of the tip-sample interaction with the nanoscale tip in contact with silicon oxide residing on a doped silicon semiconductor is given. Doped silicon with an oxide layer on top of it is a typical measurement sample for SMM and often the question arises how thick the oxide can be in order to do proper SMM measurements. Three different oxide layer thicknesses were modeled (10nm, 20nm, and 50nm) and the electromagnetic field distribution was calculated at a single frequency of 10GHz. The field distribution was plotted by using the advanced visualization capabilities to place arbitrary cutting planes within the geometrical model. Here, the total magnitude of the electrical field (i.e., the geometric sum of x, y, and z components) is plotted in logarithmic color code.

The oxide can be considered as dielectric material with only capacitive contribution and therefore most of the field decays in the oxide layer. From the electric field distribution and corresponding complex impedance values, it is evident that oxide layers of up to 20nm thicknesses can be properly used with a standard SMM tip (tip diameter <100nm). However, on oxides with 50nm thickness or more, the SMM tip field concentration is typically not sufficient to provide good SMM imaging capabilities. Furthermore, EMPro modeling shows that SMM tips with larger diameters can also probe semiconductors with thicker oxide and a quantitative relation

between maximum possible oxide thickness and tip diameter was established.<sup>5</sup> SMM experiments were done with two different tips (i.e., 20nm and 120nm tip diameters, respectively) to verify the EMPro modeling results.

Figure 5 shows a second application example of the use of EMPro in combination with SMM. Two different Pt-SiO<sub>2</sub> cross-structure samples grown on silicon wafer using focused ion beam (FIB) assisted chemical vapor deposition were imaged with SMM and analyzed with EMPro.

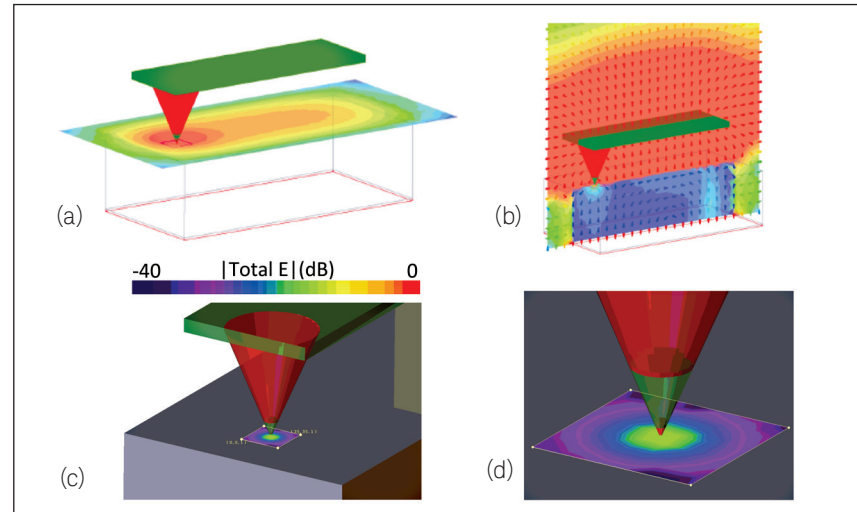


Figure 3. Electric field distribution of the AFM cantilever in contact with a sample. The sample is a three-layer stack including a metal layer at the bottom, a doped silicon chip of 500 $\mu$ m thickness, and a 50nm oxide layer of smaller lateral dimensions. (a) The electric field distribution is shown in the lateral direction on the silicon surface. (b) The field distribution is plotted onto a vertical plane with arrows and a logarithmic color scale. In (c) and (d), the field distribution is shown on the oxide surface. Information about the lateral and vertical tip-sample interaction volume can be derived. In contrast to (a) and (b), the plotted field data is drawn by a surface field sensor that can be assigned to any component surface in EMPro.

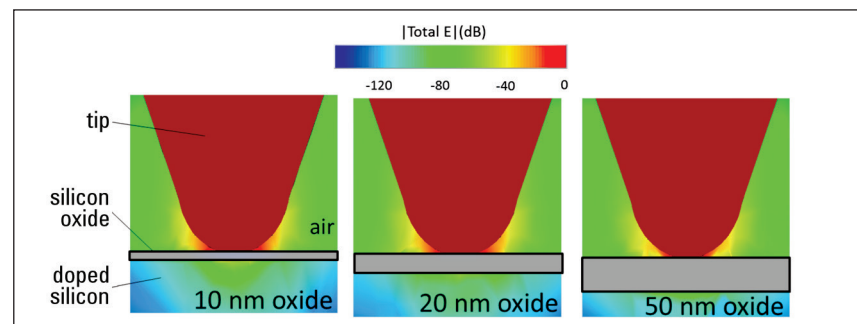


Figure 4. EMPro application example of the nanoscopic tip in contact with different layers of oxide on a semiconductor material. Three different thicknesses of an oxide layer on top of doped silicon with the probe tip directly in contact with the oxide were investigated. Oxide thicknesses are 10nm (left), 20nm (center), and 50nm (right). The local field strength at the doped silicon semiconductor surface decreases with increasing oxide thickness. At 50nm oxide thickness the electric field is already very weak, which makes standard SMM experiments difficult.

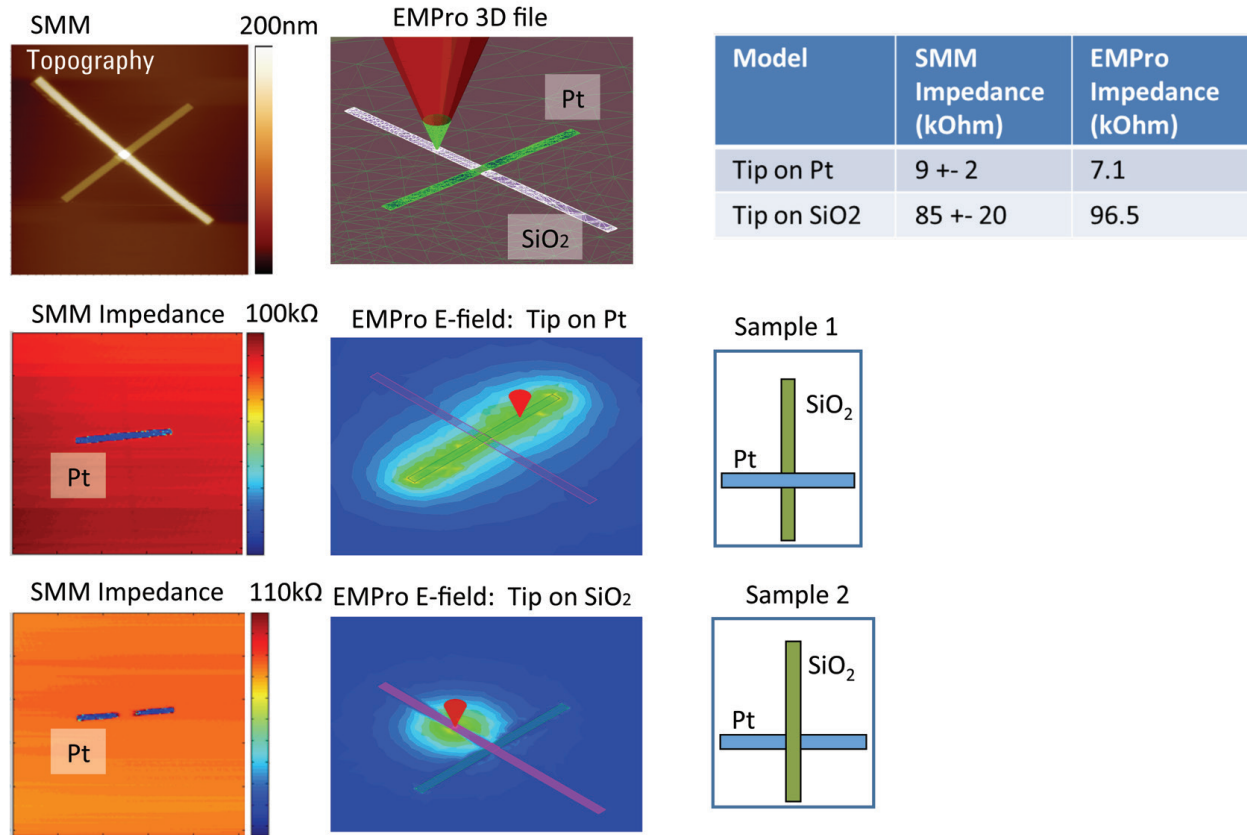


Figure 5. EMPro application example on Pt-SiO<sub>2</sub> cross-structures. Upper row: The SMM topographical image of a Pt-SiO<sub>2</sub> cross-structure is shown (left). The Pt bar has a length of 20μm, while the SiO<sub>2</sub> has a length of 30μm. The width of both bars is roughly 1μm and the height is around 20–50nm. The cross-structure geometry was imported into EMPro and the cantilever was added (center). The table compares the magnitude of the complex impedance values from the SMM measurement and the EMPro simulations (right). Center row: SMM impedance image (left) and corresponding EMPro E-field distribution (center) with the tip in contact with the Pt metal. In this sample, the Pt bar is above the SiO<sub>2</sub> bar (right). Lower row: SMM impedance image (left) and corresponding EMPro E-field distribution (center) with the tip in contact with the SiO<sub>2</sub> bar. In this sample, the Pt bar is below the SiO<sub>2</sub> bar (right).

In the first sample, the Pt bar is above the SiO<sub>2</sub> bar (Figure 5, center row) while in the second sample the Pt bar is below the SiO<sub>2</sub> bar (Figure 5, lower row). The SMM measurements show the tip-oxide impedance being significantly larger (85kOhm) than the tip-metal impedance (9kOhm). While the metal bar is continuously seen in the SMM impedance image when it is above the oxide bar, it is divided into two parts by a gap when the oxide bar is above the metal bar. In the gap region, the tip doesn't form an electrical contact with the metal bar and the larger SiO<sub>2</sub> impedance is measured. While the SMM images show complex impedance values, EMPro simulations give both complex impedance values and the corresponding 3D E-field distribution.

Firstly, the impedance values from EMPro agree well with the SMM impedance

results (cf. table in Figure 5). Secondly, the E-field distributions support the interpretation of the SMM measurements. When the tip is in contact with the metal bar, the metal virtually increases the effective tip area and the full metal bar acts as an electrode in the frame of a parallel plate capacitor. Therefore, the impedance is low when the tip is in contact with the metal, and the E-field is present along the full metal bar. It is important to point out that even when the tip is located at one end of the metal bar, the same E-field is also acting on the other end of the metal bar, and the E-field is homogeneously distributed over the full metal bar. This is nicely shown in the EMPro image of Figure 5, center row.

The situation is different when the tip is in contact with the oxide bar. Here, the actual AFM tip defines the electrode area

and the corresponding E-field is located only around the AFM tip (Figure 5, lower row). Therefore, the corresponding tip-oxide impedance values are larger because the AFM tip electrode area is smaller than the area of the Pt bar. The reduced impedance on the metal can be understood quantitatively by the following formula:  $Z = R + 1/(i\omega C)$ , with  $Z$  the complex impedance,  $R$  the resistance,  $i$  the imaginary unit,  $\omega$  the circular frequency, and  $C$  the capacitance. On the metal,  $C$  is defined by the total bar area, which is by orders of magnitude larger than the effective tip area that defines  $C$  on the dielectric oxide bar. The above mentioned analysis can also be used to investigate the complex permittivity and dielectric constants of various oxide materials, polymer matrices, and biomaterials.

## Summary

In EMPro, a simple SMM example project is included. It consists of a parameterized AFM tip in contact with a three-layer stack sample. The geometry and complexity of the sample can be easily changed within EMPro and complex impedance values can be derived for different sample geometries. Furthermore, using EMPro, the 3D E-field distribution can be calculated, which has shown to be useful for the interpretation of SMM experiments on oxide layers with different thicknesses. The complex impedance values can be compared to experimental SMM measurements as highlighted for the capacitance calibration sample and the cross-structure sample. SMM experiments result in calibrated complex impedance data, including capacitance and resistance images with nanoscale resolution down to 10nm. SMM measurements can be done on a wide range of samples, spanning semiconductor technology, materials science, and life science (including cells and membranes).

EMPro modeling can assist in the interpretation of SMM experiments and lead to a more detailed understanding of the underlying electromagnetic field distribution as well as corresponding physical properties like complex impedance, permittivity, and permeability. EMPro software efficiently complements SMM analysis software and allows more detailed investigations regarding 3D sample geometry, AFM tip diameter and shaft angle, and measurement frequency. Also, advanced SMM imaging modes and tip-sample retraction curves can be modeled and investigated in more detail using EMPro.

## Acknowledgements

For technical discussion, we would like to thank Jan Vanhese, Matt Richter, Hassan Tanbakuchi, Greg Peters, Matthias Fenner, and Manuel Moertelmaier from Keysight Technologies; Holger Arthaber and Oliver Huber from Vienna Technical University; and Prof. Ruediger Berger, Uwe Rietzler, and Maria Untch from Max Planck Institute in Mainz for providing the cross-structure samples; and Abiola Oladipo from University College London for discussions on the EMPro-SMM simulations.

## References

1. J. VanHese, J. Sercu, D. Pissort, H.-S. Lee, "State of the art in EM software for microwave engineers", Keysight Technologies Application Note 5990-3225EN, 2009.
2. J. Hoffmann, M. Wollensack, M. Zeier, J. Niegemann, H.P. Huber, F. Kienberger, "A calibration algorithm for nearfield scanning microwave microscopes", Aug. 2012, IEEE-NANO Conference Proceedings, pages 1–4.
3. H.P. Huber, M. Moertelmaier, T.M. Wallis, C.J. Chiang, M. Hochleitner, A. Imtiaz, Y.J. Oh, K. Schilcher, M. Dieudonne, J. Smoliner, P. Hinterdorfer, S.J. Rosner, H. Tanbakuchi, P. Kabos, F. Kienberger, "Calibrated nanoscale capacitance measurements using a scanning microwave microscope", Review of Scientific Instruments, 2010, vol. 81, pp. 113701.
4. H.P. Huber, I. Humer, M. Hochleitner, M. Fenner, M. Moertelmaier, C. Rankl, A. Imtiaz, T.M. Wallis, H. Tanbakuchi, P. Hinterdorfer, P. Kabos, J. Smoliner, J.J. Kopanski, F. Kienberger, "Calibrated nanoscale dopant profiling using a scanning microwave microscope", Journal of Applied Physics, 2012, vol. 111, no. 1, pp. 014301.
5. A. Oladipo, M. Kasper, S. Lavdas, G. Gramse, F. Kienberger, N. C. Panou, "Finite element simulations of a volumetric scanning microwave probe for imaging at the nanoscale", Conference Proceeding Meta-materials 2013.

For more information on Keysight Technologies' products, applications or services, please contact your local Keysight office. The complete list is available at: [www.keysight.com/find/contactus](http://www.keysight.com/find/contactus)

### Americas

Canada	(877) 894 4414
Brazil	55 11 3351 7010
Mexico	001 800 254 2440
United States	(800) 829 4444

### Asia Pacific

Australia	1 800 629 485
China	800 810 0189
Hong Kong	800 938 693
India	1 800 112 929
Japan	0120 (421) 345
Korea	080 769 0800
Malaysia	1 800 888 848
Singapore	1 800 375 8100
Taiwan	0800 047 866
Other AP Countries	(65) 6375 8100

### Europe & Middle East

Austria	0800 001122
Belgium	0800 58580
Finland	0800 523252
France	0805 980333
Germany	0800 6270999
Ireland	1800 832700
Israel	1 809 343051
Italy	800 599100
Luxembourg	+32 800 58580
Netherlands	0800 0233200
Russia	8800 5009286
Spain	800 000154
Sweden	0200 882255
Switzerland	0800 805353
	Opt. 1 (DE)
	Opt. 2 (FR)
	Opt. 3 (IT)
United Kingdom	0800 0260637

For other unlisted countries:  
[www.keysight.com/find/contactus](http://www.keysight.com/find/contactus)  
 (BP-09-23-14)

myKeysight

myKeysight

[www.keysight.com/find/mykeysight](http://www.keysight.com/find/mykeysight)

A personalized view into the information most relevant to you.

